Vortex Motion in High-T_c Films and a Micropattern-induced Phase Transition

R. Wördenweber[1], E. Hollmann[1], J. Schubert[1], R. Kutzner[1], and Ajay Kumar Ghosh[1,2]

[1]Institut für Bio- und Nanotechnologie (IBN) and JARA-Fundamentals of Future Information Technology , Forschungszentrum Jülich , D-52425 Jülich, Germany

[2]Department of Physics, Jadavpur University, Kolkata 700 032, India

E-mail: r.woerdenweber@fz-juelich.de

Abstract - **A micropattern-induced transition in the mechanism of vortex (magnetic flux quantum) motion and vortex mobility is observed in high-T_c thin films. The competition between the anomalous Hall effect (AHE) and the guidance of vortices by rows of micro-holes (antidots) lead to a sudden change in the direction of vortex motion that is accompanied by a change in the critical current density and microwave losses. The latter effect demonstrates the difference in vortex mobility in different phases of vortex motion in between and within the rows of antidots.**

I. INTRODUCTION

The dynamics of magnetic flux quanta (vortices) in superconductors shows similarity with that of quanta of electrical charge (electrons) in solids [1]. Exploring ways to control the motion of vortices has turned out to be useful for the understanding of vortex physics, for the improvement of existing superconducting devices, and for the development of innovative fluxtronic devices that employ vortices instead of electrons. Superconductors with periodic arrangements of pinning centres are suitable systems for studying dynamic phenomena of vortex movement. Beginning with the demonstration of commensurability effects in superconducting thin films with regular arrays of sub-μm holes (antidots) serving as artificial defects [2-6], we could demonstrate that local vortex trapping and guidance of magnetic flux motion can be achieved via strategically positioned antidots and antidot arrays [7,8]. Appropriate periodic antidot structures breaking the symmetry of the vortex pinning potential [8-11] resulted also in vortex ratchet effect, observed in both low- and high-T_c thin films [12]. This effect suggests the feasibility of more complex fluxtronic device concepts. In all these concepts, the manipulation of vortices via patterning will be essential.

The purpose of our work presented here was to investigate the possibility of inducing a transition from unguided to guide vortex motion within suitably patterned high-T_c thin films. We demonstrated that a properly designed arrangement of arrays of antidots in high-T_c films can lead to guided vortex motion that sets in at a clearly defined temperature. The inversion of the longitudinal component of vortex motion and the resulting change in the mobility of vortices were demonstrated via combined dc and microwave measurements.

II. SAMPLE PREPARATION, DESIGN and EXPERIMENTAL TECHNIQUES

We deposited high-T_c films of $YBa_2Cu_3O_{7-\delta}$ (YBCO) via pulsed laser deposition or magnetron cathode sputtering on microwave-compatible substrates of either $LaAlO_3$ or CeO_2-buffered sapphire. The CeO_2 buffer layers had a thickness of ~30nm. For YBCO we chose a film thickness of $d \approx$ 50-100 nm to obtain a large effective penetration length and low critical currents. The latter property is important to avoid local heating, especially at contact pads during flux flow experiments. The zero-temperature effective penetration depth $\lambda_{eff} = \lambda_L$ coth(d/2λ_L) [13] is about ~1.4μm to ~0.7μm in our 50 to 100 nm thick YBCO films. The lattice mismatch between YBCO and the substrate (2% for $LaAlO_3$ and 10-12% for r-cut sapphire) resulted in a slight reduction of the transition temperature. T_c values range from 88 to 89K for YBCO on sapphire.
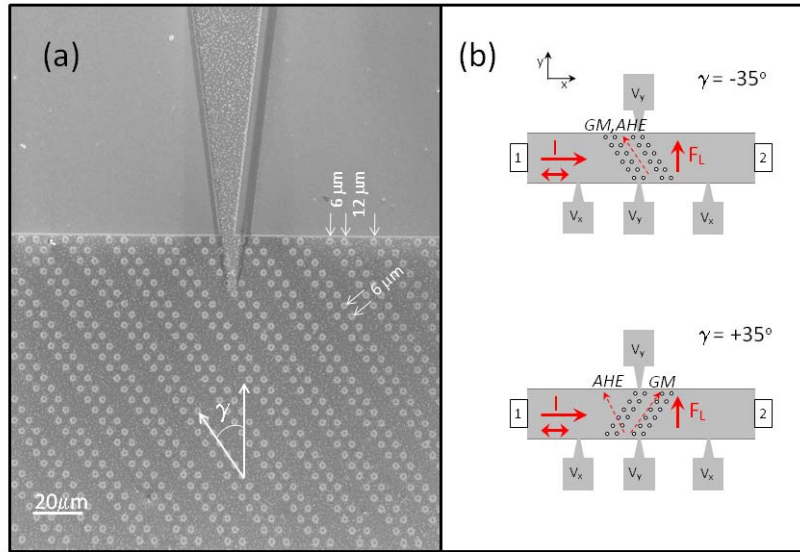

Fig.1. (a) Microscopic image of a section of a sample depicting one of the Hall contacts and the configuration of antidot rows. (b) Schematics of sample design with two different orientations of rows: γ = -35° and γ = +35°. The angle γ is defined by the nominal direction of the Lorentz force and the orientation of rows. The voltage probes, input and output ports for dc and rf current (1, 2), the directions of current, Lorentz force, anomalous Hall effect (AHE) and guided motion (GM) are shown.

To guide vortices, arrays of small holes (antidots) were patterned in our films via optical lithography and ion beam etching. In experiments discussed here, pairs of parallel rows of antidots having the nominal diameter of 1.2±0.05 μm have been used. The spacing of antidot centers in each row pair was 6 μm, the distance of adjacent antidot centers between neighboring row pairs was ~12 μm, as shown in the microscopic image of Figure 1. Inset in that figure shows schematically the sample design. The film strip along x axis can serve as a stripline for microwave signals. In superconducting state, when dc current I is applied along the x axis of the sample (at ports 1 and 2), and $d << \lambda_{eff}$, the Lorentz force F_L perpendicular to I acts on the vortices along the y axis. With decreasing temperature T, $F_L(I)$ increases and

simultaneously the strength of vortex-antidot interaction increases too. Below a certain temperature they will move along each row. We chose the angle γ between the row direction and the y axis to optimize the Hall signal voltage V_y due to guided motion of vortices. According to the simplified "1-channel model" [8], in which the flux is expected to drift predominantly along the row of antidots, the component of the Lorentz force, which compels vortices to move along the antidot rows (i.e. guided motion), is $F_{guid} = F_L \cos\gamma$, where F_L is the modulus of the Lorentz force $F_L = |\mathbf{F}_L|$. In turn, it is the component of F_{guid} parallel to the applied current, $F^{//}_{guid} = F_{guid} \sin\gamma = F_L \cos\gamma \sin\gamma$, which contributes to the Hall voltage and finally leads to the Hall signal $V_{Hall} \propto F_L \cos\gamma \sin\gamma$. The experimentally determined angular dependence of V_{Hall} roughly obeys this simple relation. specifically, the maximum Hall voltage is obtained for $\gamma = 30^o$ to 40° [14,15] while the 1-channel model predicts a maximum at 45° [8]. We thus fabricated and characterized two sample types, one with $\gamma = +35^o$, and another with $\gamma = -35^o$.

We analyzed critical dc properties of our films and the vortex dynamics in the superconducting state, between approximately $T = 82$ K and T_c, via combined resistive and microwave 6-probe measurements. A microwave signal in the frequency range between 0.05 to 20 GHz, with up to 5 dBm maximum input power, was superposed on the dc current applied to the superconducting stripline. The current (dc and microwave) was inserted at ports 1 and 2 (see Figure 1). The microstrip and the ports were 50 Ω impedance-matched. The voltage contacts were small in size and designed to minimize microwave penetration into the dc measurement setup. The longitudinal and transverse (*i.e.*, Hall signal) components of the dc voltage, V_x and V_y, characterized the transverse ($<v_y>$) and longitudinal ($<v_y>$) components of vortex motion velocity. The microwave transmission coefficient S_{21} was simultaneously recorded to provide a measure for losses resulting from vortex motion. The dc voltages were measured by Keithley nanovoltmeter 181. The Hewlett Packard network analyzer HP8720D was used to measure S_{21}. Low-intensity dc magnetic fields were applied normal to the film surface using normal Helmholtz coils to generate vortices. Field range up to a few mT was chosen to avoid inducing interstitial vortices between the antidots.

III. EXPERIMENTAL RESULTS AND DISCUSSION

A. *Definitions of Measured Parameters*

The longitudinal voltage represents the standard parameter to characterize the critical properties of a superconducting stripline. In the normal regime, $V_{longitudinal}$ represents the normal state resistivity, whereas in superconducting regime, it is generated by vortex motion along the Lorentz force, *i.e.*, across the stripline. In the latter case, $V_{longitudinal}$ characterizes the average velocity component $<v_y>$ of vortex, *i.e.*, is a measure for the flux transfer across the stripline collected between the longitudinal voltage contacts labeled V_x in Figure 1.

The Hall signal in superconducting regime characterizes the vortex motion along the stripline. The chosen arrangement of Hall contacts (labeled V_y in Figure 1) makes possible the analysis of the component of vortex motion parallel or antiparallel to the current. Furthermore, it enables a more local analysis of the vortex motion that is restricted to the vicinity of the contacts pair. High-T_c materials typically reveal the, so-called, anomalous Hall effect (AHE), *i.e.*, the sign inversion of the Hall signal below T_c [14,16-24]. It has been shown, that the AHE in high-T_c material is caused by vortex motion. Most likely the

additional component of vortex motion is caused by the Magnus force acting on the very weakly pinned vortices, close to T_c [14]. Depending on the orientation of the rows of antidots, the AHE can be suppressed or not. This is demonstrated in Figure 2. It shows the transition to the superconducting stated determined by the measurements of the longitudinal voltage together with the temperature dependence of the Hall signals for both designs $\gamma = +35^o$ and $\gamma = -35^o$. Whereas the Hall contacts positioned at antidots rows with $\gamma = +35^o$ display the AHE, the Hall signal measured at antidots rows with orientation $\gamma = -35^o$ do not show signs of an AHE[*].
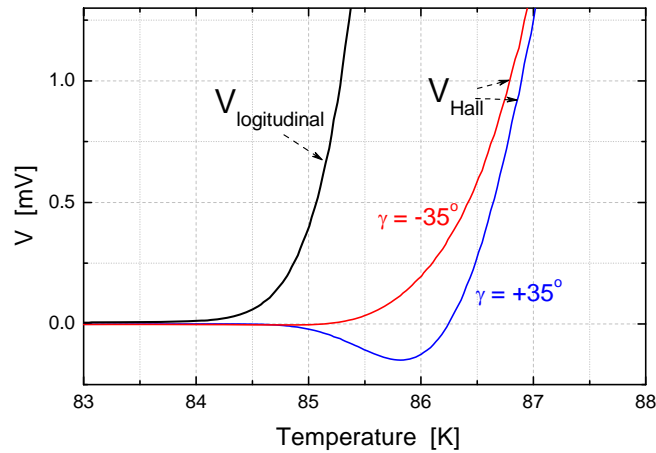

Fig. 2. Temperature dependence of the longitudinal voltage (contacts V_x) and Hall signals (contacts V_y) at the transition temperature. Depending on the direction of rows of antidots contacts the anomalous Hall effect is present ($\gamma = +35^o$) or suppressed ($\gamma = -35^o$).

Additionally to the transition temperature, the critical current density J_c can be recorded via the different contacts. The standard J_c value is defined by measurements of the longitudinal voltage (voltage contacts V_x). The longitudinal voltage is kept constant (typically at a value of a voltage criterion of a few μV/cm) and the resulting current defines the critical current I_c.= $J_c \cdot d \cdot w$ (d and w represent the thickness and width of the stripline). For our samples, $J_c(T)$ shows the classical behavior for both arrangements of rows of antidotes (with positive and negative angle γ). Except for temperatures near the transition from normal state, J_c increases linearly with decreasing temperature.

Similar to measurements of the classical critical current, we could keep the component of vortex motion $\langle v_x \rangle$ constant by controlling the Hall signal. This way, the critical current density $J_{c,Hall}$ is defined in analogy to the classical critical current density J_c defined by the longitudinal voltage. The advantage of the definition of $J_{c,Hall}$ is that a defined component of

---

[*] Please note, that the longitudinal voltage collects the total flux transport across the stripline registered between the voltage contacts V_x whereas the Hall signal records the vortex motion 'across the imaginary line between each pair of Hall contacts V_y'. Consequently, the longitudinal voltage signal is orders of magnitudes larger compared to the Hall signal for the case of vortex motion. Therefore a finite signal $V_{longitudinal}$ persists to lower temperatures where the Hall signal is already so small that it cannot be measured.

vortex motion perpendicular to the Lorentz force is established. This component of motion can only be due to additional forces, like the Magnus force or the guidance force. Therefore $J_{c,Hall}$ is more suitable to characterize properties related to these forces than the classical definition of J_c.

B. Hall Critical Voltage and Current versus Temperature

Figure 3 shows the plots of critical current densities $J_{c,Hall}$ for both orientations of rows of antidots in a small applied magnetic field of 0.6 mT. To obtain a high mobility of vortices a large voltage criterion was chosen for these measurements, $|V_{c,Hall}| = 100\mu V$. Due to the larger voltage criterion J_{cHall} is larger than J_c. Nevertheless, the overall functional dependencies of J_c and $J_{c,Hall}$ are the same for both orientations of antidot rows, except for the behavior of the sign of the critical voltage (direction of vortex motion) and a small hysteretic jump in J_{cHall} for one of the orientations of antidot arrows. This will be discussed below.
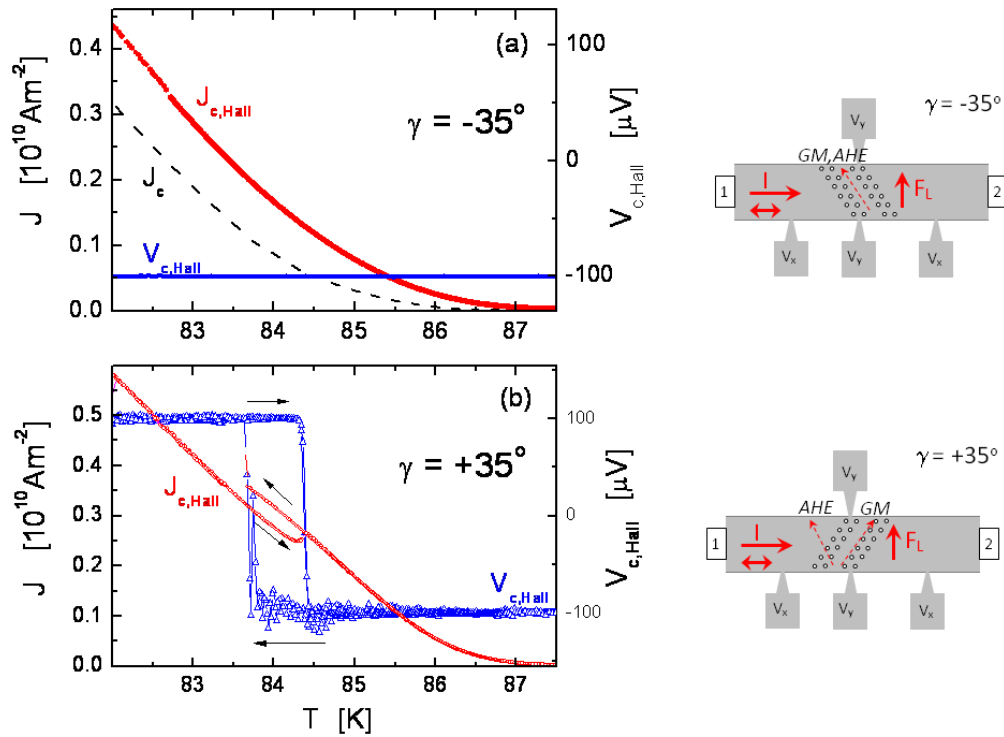

Fig. 3. Left side: critical current densities $J_c(T)$ (black dashed line, voltage criterion $V_c=5\mu V/cm$) and $J_{c,Hall}$ (T) (red plot) for two different orientations of rows: $\gamma = -35^o$ (a) and $\gamma = +35^o$. $J_{c,Hall}$ is defined by a Hall voltage $|V_{c,Hall}|=100\mu V$ (blue triangles). The arrows indicate the direction of temperature change during the experiment, the magnetic field was 0.6mT. Right side: the corresponding sample configurations from Fig. 1.

(i)   When $\gamma = -35^\circ$, Figure 3 (a), the Hall signal was negative over the whole investigated temperature range below T_c, the vortices moved in the direction of rows, indicated by the dashed red arrow in the inset of Figure 3 (a). The value of $J_{c,Hall}$ (corresponding to $V_{c,Hall} = -100\mu V$) increased monotonically with decreasing temperature. It agreed qualitatively with the behavior of the critical current J_c in the superconducting state (black dashed line). The quantitative difference between J_c and $J_{c,Hall}$ is explained by differences in the voltage criteria ($V_c = 5\mu V/cm$ and $|V_{c,Hall}| = 100\mu V/cm$) and the different components of vortex motions (parallel or antiparallel to the Lorentz force) that are characterized.

(ii) When $\gamma = +35^\circ$, Figure 3 (b), a different vortex behavior is observed. The Hall voltage changes sign when cooling down from T_c. A negative voltage is observed close to T_c, when vortices do not follow the guidance of antidot rows. However, approximately 3 K below T_c, the Hall voltage changes abruptly to a positive value. The vortices move now in the direction imposed by antidot rows. This change of direction of vortex motion is hysteretic, *i.e.*, it occurs at 83.7 K and 84.4 K for decreasing and increasing temperatures, respectively. It is accompanied by a hysteretic change in the critical current $J_{c,Hall}$, seen in Figure 3 (b), and a change of the microwave transmission coefficient S_{21} at exactly the same temperatures, as shown in Figure 5. The abrupt jump in the Hall voltage, critical current and microwave properties suggests a change of the mechanism of vortex motion in the second sample. It is discussed in the following and confirmed by microwave experiments (see below).

Close to T_c, the negative Hall voltage is indicative of the presence of the anomalous Hall effect (AHE) [14,16-24]. The vortex-antidot interaction is weak in this temperature range. Consequently, the guidance of vortex motion by the rows of antidots is negligible. The AHE dominates and vortices move in the direction defined by the AHE as indicated in sample drawings of Figures 1 and 3 (it should be noted, that only the direction but not the angle for this motion can be measured). With decreasing temperature the vortex-antidot interaction strength increases and, finally, the guidance of vortices via the rows of antidots starts to dominate the AHE. The vortices move within the rows of antidots [15].

When the orientation angle of antidot rows coincides with the direction of $<v>$ resulting in AHE, as is the case for the design of Figure 2 (a), AHE and guided motion (GM) by antidot rows point in the same direction. Therefore, the Hall voltage stays negative over the whole temperature range, and changes in the critical current density and microwave properties are monotonous functions of T. In contrast, a change of direction of motion is necessary when transition from AHE to guided motion occurs in the design of Figure 2 (b). Close to T_c vortices shuttle between the rows of antidots, while below a certain temperature they move within the rows of antidots. This implies a modification of the mechanism of vortex motion. Whereas vortices mainly travel in the superconductor in the first case, they 'hop' from antidot to antidot in the latter case. This difference in the mechanism of vortex motion is visible in the resulting jumps in the critical current density and the microwave loss. The Hall critical current is modified by 10-12% at the transition. Vortex motion within the rows of antidots seems to be energetically more favorable than it is in the superconducting matrix. This agrees with results obtained from imaging of vortex motion in microstructured YBCO films [15]. Thus, the guidance of vortices by antidots is based on the reduction of the potential barrier for vortex motion along the row of antidots.

C. Microwave Properties

Microwave transmission properties can provide information on the mobility of vortices and their residence time in the superconductor. Vortex motion contributes to losses and thus affects the transmission. Figures 4 and 5 present the measured microwave transmission coefficient, S_{21}, *versus* temperature for our two orientations of antidot rows $\gamma = \pm 35^{\circ}$. The microwave was fed to the strip line via port 1 and 2, the frequency in this experiment was 4 GHz, and magnetic field of 1.6mT was applied. Generally, the transition to the superconducting state (at $T_{c} \approx 88.5$K) leads to a steep increase of S_{21}, because the microwave surface resistance in the superconducting state is reduced. Below T_{c}, S_{21} depends on the driving force acting on vortices. This driving force can be supplied by the dc current or the microwave current.

In Figure 4 the applied microwave power is varied. In the superconducting regime, losses increase with the microwave input power at the sample. Therefore, the difference between transmission parameters ΔS_{21} recorded at two different values of input power (–5 and –25 dBm) is also plotted. Obviously, ΔS_{21} is zero in the normal regime. In the superconducting regime largest mobility of vortices is present closed to T_{c} thus leading to the dip in $-\Delta S_{21}$. With decreasing temperature, vortex pinning increases and $-\Delta S_{21}$ decreases.
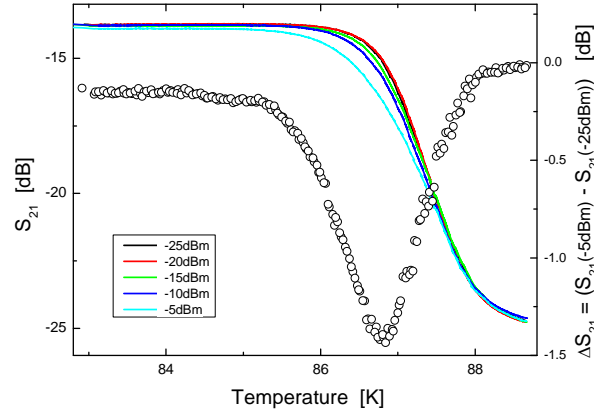

Fig.4. Temperature dependence of the transmission parameter S_{21} measured for different microwave powers at 4GHz and 1.6mT on stripline with $\gamma = -35^{\circ}$. The difference ΔS_{21} between the transmission parameters S_{21} obtained for -5 and -25dBm is given.

Figure 5 shows the microwave behavior of the sample with $\gamma = +35^{\circ}$. The transmission coefficient *versus* temperature is determined at a constant microwave power (-17dBm) for two values of dc current: $J_{dc} = J_{c,Hall}$ and $J_{dc} = 0$. Due to the low microwave power applied, we can analyze the mobility of moving vortices ($J_{dc} = J_{c,Hall}$) or stationary vortices ($J_{dc} = 0$). Similar to the observation in Figure 4, the transition to the superconducting state at $T_{c} \approx 88.5$K leads to a steep increase of S_{21} due to the strong reduction of the microwave surface resistance in the superconducting state. Below T_{c}, S_{21} is dependent on the vortex motion. At lower temperatures (~87.4K) the ΔS_{21} determined from measurements at zero-current and critical Hall current becomes visible. Therefore, vortices are first formed at this temperature and their motion due to the applied current results in additional microwave losses. The losses increase with decreasing temperature and saturate at a value of $\Delta S_{21} \approx 2.1$dB. In this temperature regime the AHE dominates the longitudinal vortex motion, vortices shuttle between the rows

of antidots, *i.e.*, they mainly move in the superconductor. The losses due to moving vortices are relatively large. At lower temperature, the transition to guided motion via antidot rows takes place in the case of $\gamma = +35^o$. The transition causes an abrupt increase of the transmission coefficient by more than 1dB. It demonstrates that the motion of vortices within the row of antidots causes smaller losses than the motion in the superconducting matrix. On the one hand, this is unexpected. The motion of vortices between antidots will cause a temporary local switching to the normal state of the area between the antidots. Since the rows of antidots already represent a suppression of the current carrying cross-section one would expect an enhancement of microwave losses [15]. On the other hand, the residence time of vortices in the superconductor is shorter for guided motion than for vortices travelling in the superconducting matrix. This effect could even be enhanced by a hopping like motion, where the vortices rapidly jump between antidots and remain longer in the antidots. This hopping like motion would agree with simulations of vortex motion in arrays of antidots [25]. In this temperature regime, the impact of vortex motion on microwave losses decreases with temperature. Finally at $T < 82K$, $\Delta S_{21} \approx 0$, *i.e.*, vortex motion has no effect on microwave losses any more. In contrast to the situation for decreasing temperatures, the transition back to AHE dominated vortex motion with increasing temperature occurs gradually. It seems that guidance is switched off individually in the different double rows.

In closing, we note that apparent discrepancies between $S_{21}(T)$ plots in Figure 4 and those of Figure 5 can be explained by the difference in the vortex driving force strength caused by dc and microwave current. The applied microwave energy range of Figure 4 (microwave current only) is low enough not to cause noticeable vortex motion. Therefore, the plots for this range coincide at lower temperatures, below 85.5 K approximately. In Figure 5 (dc and microwave current), the dc current driving force is stronger, so $S_{21}(T)$ plots merge at the temperature of less than 83 K.
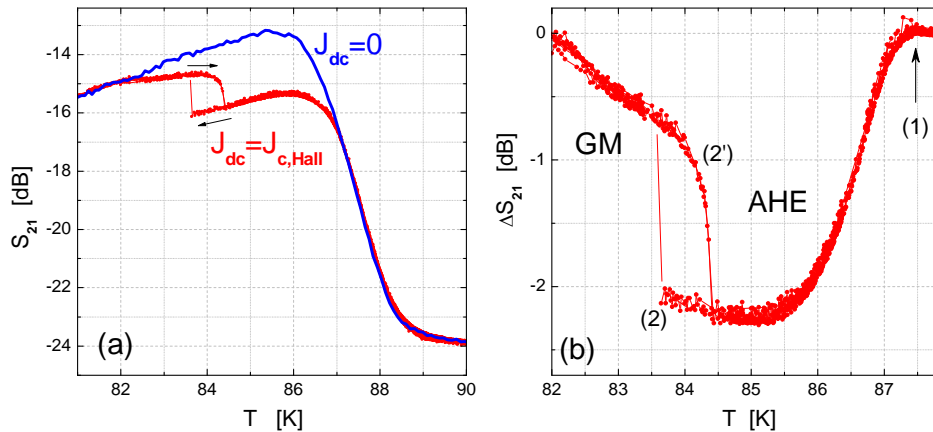

Fig. 5. Temperature dependence of the microwave transmission coefficient S_{21} of the design shown in Fig. 3(b) (γ=+35°) for dc current densities J=0 and $J = J_{c,Hall}$ (a) and difference of S_{21} obtained for both currents (b). The data are recorded at a frequency of 1GHz, rf-power of -17dBm at the sample and a magnetic field of 0.6mT. The positions 1,2 and 2' mark the onset of vortex nucleation and phase transitions of vortex motion, respectively.

IV. CONCLUSION

In conclusion, we demonstrated that a transition in the vortex motion and vortex mobility can be induced by appropriate antidot structures micropatterned in superconducting thin films. The competition between the AHE and the guidance of vortices by rows of antidots leads to a simultaneous change in the sign of the Hall voltage, in the critical current density and microwave transition coefficient. Close to T_c, the AHE dominates and vortices shuttle between the rows, whereas at lower temperatures the vortices are guided by rows of antidots. Microwave measurements demonstrate the difference in vortex mobility in these two different regimes or "phases". The different dc and microwave experiments in combination with micropatterning of thin high-T_c superconducting film might pave the way towards strategic manipulation of vortices. Systematic analysis of manipulation methods could in turn pave the route towards interesting and innovative fluxonic effects and device concepts.

ACKNOWLEDGEMENT

REFERENCES

[1] A. Maeda, Y. Inoue, H. Kitano, *et al*., *Phys. Rev. Lett*. **94**, 077001 (2005).

[2] A. N. Lykov, *Solid State Commun*. **86**, 531 (1993).

[3] M. Baert, V. V. Metlushko, R. Jonckheere, *et al*., *Phys. Rev. Lett*. **74**, 3269 (1995)

[4] A. M. Castellanos, R. Wördenweber, G. Ockenfuss, *et al*., *Appl. Phys. Lett*. **71**, 962 (1997).

[5] M. Lange, M. J. Van Bael, Y. Bruynseraede, V.V. Moshchalkov, *Phys. Rev. Lett*. **90**, 197006 (2003).

[6] S. Raedts, A.V. Silhanek, M. J. Van Bael, V.V. Moshchalkov, *Phys. Rev*. B **70**, 024509 (2004).

[7] R. Wördenweber, A. M. Castellanos, P. Selders, *Physica* C **332**, 27 (2000).

[8] R. Wördenweber, P. Dymashevski, V. R. Misko, *Phys. Rev*. B **69**, 184504 (2004).

[9] J. E. Villegas, S. Savel'ev, F. Nori, *et al*., *Science* **302**, 1188 (2003).

[10] J. Van de Vondel, C. C. de Souza Silva, B. Y. Zhu, *et al*., *Phys. Rev. Lett*. **94**, 057003 (2005).

[11] C. C. de Souza Silva, A.V. Silhanek, J. Van de Vondel, *et al*., *Phys. Rev. Lett*. **98**, 117005 (2007).

[12] B.Y. Zhu, F. Marchesoni, F. Nori, *Phys. Rev. Lett*. **92**, 180602 (2004).

[13] K. K. Likharev, *Sov. Phys. JETP* **34**, 906 (1972).

[14] R. Wördenweber, J.S.K. Sankarraj, P. Dymashevski, E. Hollmann, *Physica* C **434**, 101 (2006).

[15] A. Lukashenko, A. V. Ustinov, A. P. Zhuravel, *et al*., *J. Appl. Phys*. **100**, 023913 (2006).

[16] S.J. Hagen, C.J. Lobb, R.L. Greene, *et al*., Phys. Rev. B **41**, 11630 (1990).

[17] S.J. Hagen, A.W. Smith, M. Rajeswari, *et al*., Phys. Rev. B **47**, 1064 (1993).

[18] P. Ao, *J. Phys. Condens. Matter* **10**, L677 (1998).

[19] H.J. Jensen, P. Minnhagen, E. Sonin, H. Weber, *Europhys. Lett*. **20**, 463 (1992).

[20] R.A. Ferrell, *Phys.Rev. Lett*. **68**, 2524 (1992).

[21]   A.van Otterlo, M. Feigel'man, V. Geshkenbein, G. Blatter, *Phys. Rev. Lett*. **75**, 3736 (1995).

[22]   D.I. Khomskii, A. Freimuth, *Phys. Rev. Lett*. **75**, 1384 (1995).

[23]   N.B. Kopnin, *Phys. Rev*. B **54**, 9475(1996).

[24]   J. Kolacek, P. Vasek, P*hysica* C **336**, 199 (2000).

[25]   C. Reichhardt, C. J. Olson, and F. Nori, Phys. Rev. B **58**, 6534 (1998).